Engineering Failure Analysis 97 (2019) 434–453

Contents lists available at ScienceDirect

Engineering Failure Analysis

journal homepage: www.elsevier.com/locate/engfailanal

Failure intensity of offshore power plants under varying maintenance policies

Lokukaluge P. Perera[a,*], Mario M. Machado[b], Anders Valland[c], Diego A.P. Manguinho[b]

[a] UiT The Arctic University of Norway, Tromso, Norway
[b] Petróleo Brasileiro SA, Rio de Janeiro, Brazil
[c] SINTEF Ocean, Trondheim, Norway

ARTICLE INFO

Keywords:
System reliability
Failure rates
Failure intensity
Gas turbine engines
Nonhomogeneous Poisson process

ABSTRACT

System reliability of an offshore power plant with several gas turbine engines is analyzed in this study to understand the failure intensity of a selected gas turbine engines under varying maintenance activities. A set of event data of a selected gas turbine engine is considered to identify system failure intensity levels, where unknown maintenance actions were implemented (i.e. various repairs disturb the failure rate). A non-homogeneous Poisson process (NHPP) is used to model the age dependent failure intensity of the same gas turbine engine and the maximum likelihood estimation (MLE) approach for calculating the respective model parameters is proposed. Several failure intensity rates (i.e. varying failure trends) in these models (i.e. during the system age of the gas turbine engine) are observed. Furthermore, these varying failure trend models are evaluated with actual failure events of the same gas turbine engine by considering two goodness-of-fit tests: Cramer-von Mises and Chi-square tests. Finally, system reliability of the gas turbine engine under the failure transition, failure intensity, mission reliability and mean time between failures (MTBF) is also discussed in this study.

1. Introduction

1.1. Oil and gas industry

Oil & gas production recovery rates have been increased in the recent years due to various technological advancements in the offshore industry. Since a considerably lower amount of new investments are going into this industry, the present oil and gas infrastructure has been enforced to cope with these challenging operational requirements due to extended petroleum production activities. Therefore, the current production requirements to operate the same facilities beyond their design life are considered by the oil and gas industry. It is expected that these offshore platforms should continue their operations with appropriate maintenance actions under the required structural integrity and system safety levels beyond their design lives [1]. Furthermore, new structural and system upgrades should be initiated to improve the operational reliability in such offshore platforms. The operational reliability in the oil and gas industry can be categorized under three main considerations [2,3]: availability (i.e. production conditions), safety (i.e. risk analysis, safety systems availability) and maintainability (i.e. critical analysis, life cycle cost, life extensions). However, the oil

* Corresponding author.
E-mail addresses: prasad.perera@uit.no (L.P. Perera), mmarcondes@petrobras.com.br (M.M. Machado), anders.valland@sintef.no (A. Valland), diegomanguinho@petrobras.com.br (D.A.P. Manguinho).

https://doi.org/10.1016/j.engfailanal.2019.01.011
Received 27 February 2018; Received in revised form 24 November 2018; Accepted 2 January 2019
Available online 06 January 2019

Nomenclature

$C_M{}^2$	The value of the Cramer-Von Mises goodness-of-fit test
E[.]	The expectation function
H_i	The ith hypothesis
$L(.)$	The likelihood function
$\widehat{M}(.)$	The estimated mean time between failures
$N(.)$	The number of system failures
N_d	The number of data intervals of the Chi-square test
N_i	The observed number of system failures in ith data intervals of the Chi-square test
n_i	The number of failures during the time period $(t_{i-1}\ t_i]$
$\bar{n}$	The number of time periods,$(t_{i-1}\ t_i]$, during the operational period T
P[.]	The probability function
P_π	The π-th $\left(\pi \approx 1 - {}^{\alpha}/_{2}\right)$percentile for a normal distribution with mean 0 and variance 1
$R(.)$	The mission reliability
t, t_i	The system age
T	The operational period
(T_{Si}), T_S	The (ith) starting system age at the operational period T
(T_{Ei}), T_E	The (ith) ending system age at the operational period T
X_i	The time period for the ith system failure (from $t = 0$)
U_L	The value of the Laplace trend test
α	The significance level
$\beta, \widehat{\beta}$	The actual and estimate system parameters of the NHPP ($\beta > 0$)
β_{LB}, β_{UB}	The approximate $(1-\alpha)\cdot 100$ percent lower and upper confidence bounds for β
$\overline{\beta}$	The unbiased estimator for β
γ	The significance level
$\widehat{\theta}_i$	the expected number of failures in the i-th data interval of the Chi-square test
$\lambda, \widehat{\lambda}$	The actual and estimated system parameters (i.e. Failure rate) of the NHPP ($\lambda > 0$)
$\lambda_{LB}, \lambda_{UB}$	The approximate $(1-\alpha)\cdot 100$ percent lower and upper confidence bounds for λ
$\mu(.)$	The system failure intensity
Π_1, Π_2	The designated confidence coefficients for the two sided $(1-\alpha)\cdot 100$ percent confidence intervals of the MTBF
χ^2	The value of the Chi-square test
$\chi_{MLE}{}^2$	The value of a Chi-square distribution in maximum likelihood estimation (MLE)
ω	A statistical distribution approximately a normal distribution with mean 0 and variance 1

and gas industry is struggling to identify critical operational reliability requirements for aging offshore facilities under appropriate cost-effective maintenance actions.

This study focuses on quantifying the operational reliability of an offshore power plant with several gas turbine engines as the main contribution. Since offshore power plants play a crucial operational role in the oil and gas industry, in which consist of various engine-power configurations to satisfy the power requirements and improve the availability of offshore operations. Such engines are operating under harsh ocean environmental conditions, therefore condition monitoring (CM) and conditions based maintenance (CBM) approaches have often been implemented. On the other hand industrial power plants are life critical systems in aging offshore platforms. Therefore, the failure behavior (i.e. failure rate and failure intensity) on such offshore power plants, based on CM data, can be used to overcome the respective diagnostic and prognostic challenges and evaluate the success in the past and present maintenance policies. That, i.e. diagnostic and prognostic challenges and evaluate to maintenance policies in offshore power plants, can be two important applications, where the outcome of this study can be used.

1.2. Gas turbine engines

A general overview of an industrial gas turbine engine with the respective systems/subsystems is presented in Fig. 1. That consists of the main systems [4]: compressor, gas generator (GG) including combustor and gas turbine (GT) and power turbine (PT); with the respective subsystems: starting system, air intake, compressor, combustion system, HP (high pressure) turbine, LP (low pressure) turbine (power turbine), starting system, accessory drive, fuel system, fire and gas protection, lubrication system, control and monitoring, exhaust, and other miscellaneous [5]. Various health management applications (HMAs) for these systems and subsystems have been developed by the aero-space under system reliability studies [6,7]. A range of parameters that should be monitored under such HMAs in aero-space and industrial gas turbine engines are presented with the respective system symptoms and fault correlations in [3]. The symptoms and fault correlations that relate to the critical components of gas turbine engines are identified under failure mode and effects analysis (FMEA) in [8]. The gas turbine engine technology used by the aerospace industry has also been adopted by the offshore industry with additional modifications, where several technological modifications against harsh ocean environmental conditions are introduced. Those modifications consist of additional sub-systems, such air filtering, acoustics, lubrication starting and wash systems [8].

1.3. Engine health management

This study forces on system reliability of offshore power plants that consist of various gas turbine engines. Therefore, the same HMAs have been used by the aerospace industry and can be adopted towards offshore power plants to improve their technical integrity, i.e. the operation risk can be reduced and the operational efficiency can be improved. An overview of such HMAs of gas turbine engines is presented in Fig. 2, where both conventional and modern approaches are summarized. The CM data are collected as

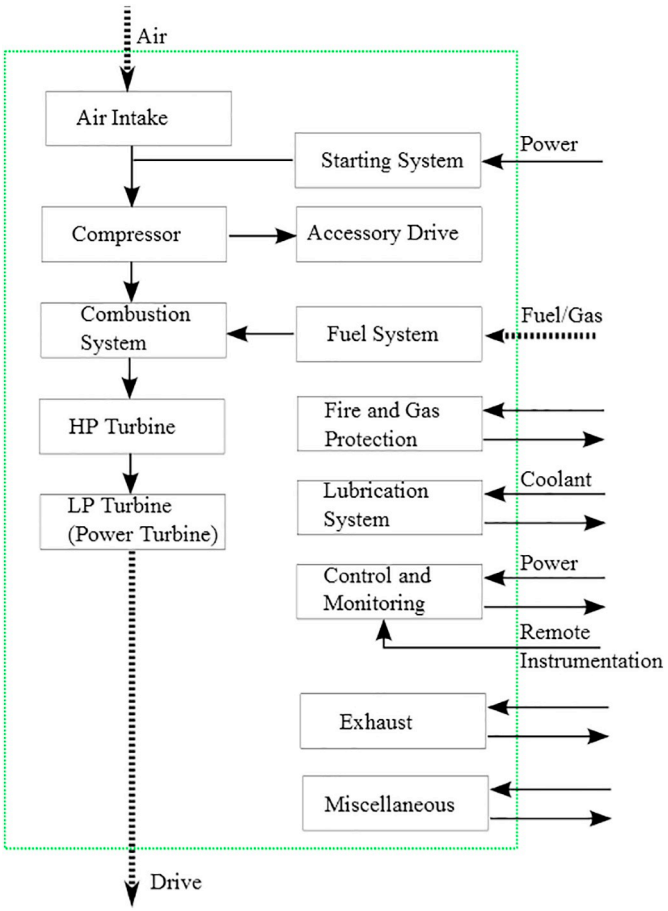

Fig. 1. Sub-systems of an industrial gas turbine engine.

real-time measurements (i.e. components pressure, temperature and speed), event data (i.e. system failure and shutdown events) and maintenance records (i.e. overhauls and repairs) in these applications. These data sets are used to develop various mathematical models for HMAs of gas turbine engines. In traditional HMAs, the mathematical models are identified by selecting a set of system states and parameters, i.e. linear or nonlinear relationships, and calculated by various estimation algorithms. Hence, estimated system states and parameters and their deviations are compared with some threshold values to evaluate the health conditions of gas turbine engines. Furthermore, appropriate estimation algorithms are used to observe unmeasurable states and parameters of gas turbine engines. The undesirable deviations of system states and parameters trigger the respective alarms. If the tolerances are exceeding the respective threshold values, such situations are identified as system degradation conditions of gas turbine engines. It is expected that critical system failures in gas turbine engines can be detected at an early stage by considering state and parameter deviations and that may prevent overall offshore power plant failures.

The mathematical models that are proposed for HMAs are summarized in this section. One should note that the initial studies on HMAs for gas turbine engines are developed by the national aeronautics and space administration (NASA), USA, to improve the air transport safety issues ([9–12]) and used for both operational and maintenance requirements [13]. That can be divided into two approaches (see Fig. 2): gas path analysis (GPA) and performance seeking control (PSC). Both approaches are used in HMAs of gas turbine engines. GPA is a diagnostic process used to observe the health conditions of gas turbine engines by observing a selected set of parameters that relate to the respective gas path components [14]. A list of the respective gas path components (i.e. steady-state station numbers, modules, and sensors) is presented in [15]. In general, these parameters consist of various component efficiencies and gas flow conditions. Those are estimated by measuring pressure, temperature and rotational speed values of the respective components of a gas turbine engine. Even though gas turbine engines operate around fixed operation points, the respective aero-thermodynamic parameters can vary due to power and ambient conditions at the engine inlet [16]. e.g. the inlet pressure and temperature values of a gas turbine engine can vary due to the environmental conditions and contribute to aero-thermodynamic parameter deviations. Hence, GPA calculations should be corrected for these variations and several parameter correction factors are introduced in [17].

PSC can be considered as an advanced version of GPA, where additional mathematical techniques [18] in system modeling, parameter estimation and control optimization are used [19]. A PSC approach, i.e. a model based real-time adaptive on-board

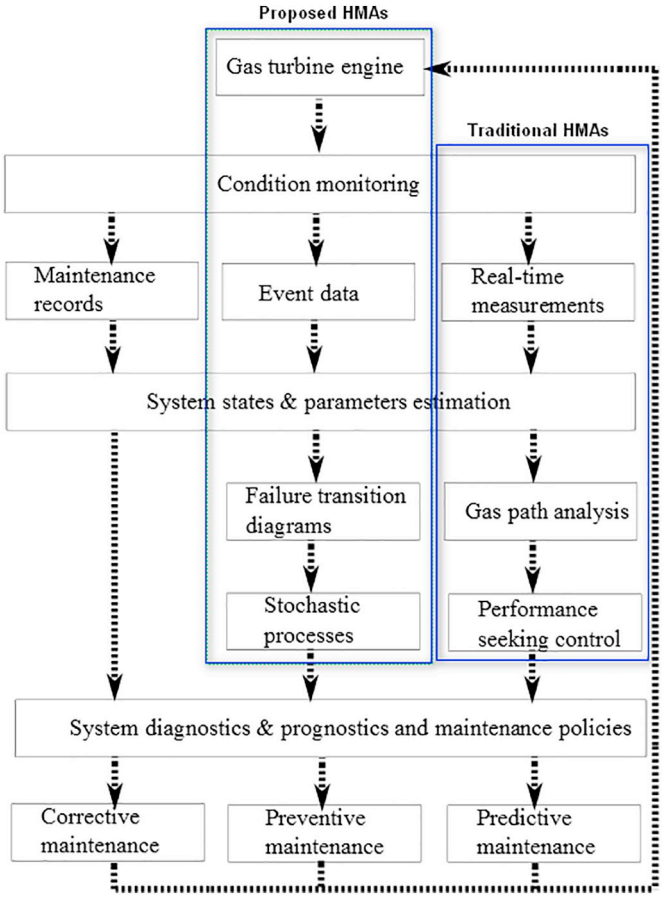

Fig. 2. Health management applications of industrial gas turbine engines.

propulsion system optimization algorithm, with inflight thrust calculations is presented in [20]. Furthermore, the same approach is expanded for optimizing aircraft performance by implementing an adaptive trim control approach in the propulsion system under a pseudo-steady-state cruise mode [21].

Both approaches (i.e. GPA and PSC) encounter various technical challenges that degrade HMAs, as summarized in this section. Firstly, the bias and variance values of measurement noise can degrade the parameter estimation process. Secondly, the health parameters may have various nonlinear relationships that cannot be observed from sensor measurements. Thirdly, a large number of sensors are required to estimate system states and parameters. Even though these challenges can partially be addressed by estimating a subset of health parameters (i.e. a reduced order mathematical model) [22] and incorporating sensor noise into estimation algorithms [23,24] with additional disturbance attention methods [25], the complexities (i.e. nonlinearities) in GPA and PSC approaches can still degrade the HMAs of gas turbine engines.

This study proposes to use system events data (see the green colored box in Fig. 2) to derive the failure behavior of gas turbine engines. The events data (i.e. failure and shutdown events) are used in the recent literature to derive the respective mathematical models in HMAs and that can be divided into two categories (see Fig. 2): failure transition diagrams and stochastic processes. Failure transition diagrams represent the probability of system transitions from one state to another during its operational period. These states may consist of various health conditions and that can be categorized as: complete operable states, operable states with minor faults, operable states with major faults, and inoperable states. One should note that various stochastic processes have been used in many HMAs for modeling the failures behavior of industrial systems [26]. The same concept is adopted in this study to estimate the system failure intensity in a selected gas turbine engine. Furthermore, stochastic process models can also be accommodated into failure transition diagrams, where the failure behavior predictions in industrial systems can be further improved. Stochastic process models with statistical methods [27] and signal processing & soft computing techniques [27] to overcome various challenges in systems diagnostics, prognostics and maintenance [28–30] of gas turbine engines are also presented in the respective literature.

1.4. Condition monitoring

Understanding the failure behavior of an offshore power plant under various system failures due to age related degradation conditions is an important part of this study. The power plant consists of several gas turbine engines and each gas turbine engine is

equipped with CM facilities. The system failure structure of gas turbines can be used to model the overall power plant behavior by considering subsystem/component faults and failure transitions (i.e. under failure transition diagrams). The historical CM data in gas turbine engines should be available to develop such system failure structures, grouped into two categories. The first category is the top-down concept, where an average engine performance trend as a function of an engine cycle is defined and that characterizes the average engine deterioration at a selected engine usage level. The second category is the bottom-up concept, where component health conditions and maintenance data can be used to determine the probable effect of the deterioration conditions of each part.

This study considers on the first category, where the average engine performance as a function of engine cycles is analyzed under the event data (i.e. CM data) of a selected gas turbine engine. Even though the second category should complement the first category, these offshore industrial platforms have not been facilitated to collect comprehensive details on component health conditions and maintenances throughout their lifetime. Therefore, the system failure intensity that has derived from the event data of a selected gas turbine engine is categorized as an average engine performance measure in this study. One should note that the system failure intensity can also be used to evaluate the present and past maintenance actions (i.e. maintenance interventions with consistence intervals) in relation to the operational costs. These operational cost calculations also relate to the engine deterioration conditions and derive from the detailed information (i.e. collected, documented and analyzed service usage data) on engine performance deteriorations, component conditions, component replacement-repair rates and maintenance practices [31]. These cost calculations can also be used to identify the most critical and expensive component failures (i.e. the most crucial system failures) of gas turbine engines by considering the respective maintenance actions and that information can be used to develop cost-effective maintenance policies.

2. System modeling

2.1. System details

An offshore industrial power plant, i.e. a floating production, storage and offloading (FPSO) unit, in Campos Basin, Rio de Janeiro, is considered in this study [32]. These FPSO units are used by the offshore industry to receive, process and store the hydrocarbons that are produced from nearby offshore platforms and sub-sea production systems. This power plant consists of 4 turbo-generators of aero-derivative gas turbine engines with normal capacity of 25,000 (kW), coupled with electric generators with normal capacity of 28,750 (kVA). These aero-derivative gas turbine engines consist of higher energy efficiency with faster star-up periods [33] and support the required gird load of the offshore platform approximately 35–45 (MW). i.e. each generator is rated approximately for 12–15 (MW). Therefore, at least 3 generators should be operated to satisfy the power requirement of the offshore platform.

2.2. System model

The CM data set from a selected gas turbine engine is considered in this section to derive an appropriate mathematical model to calculate its failure intensity. Gas turbine engines are repaired after various component failures and those system failures can be considered as stochastic events [34]. The total operational period of the gas turbine engine is denoted as $[0 \quad T]$ and that has a number of failure events of $N(T)$. It is assumed that system maintenance actions have not influenced the failure intensity of the gas turbine engine during this period, where these system failures are recovered by a same number of repairs with negligible time periods. These system failure events are considered as an independent, identically distributed (IID) random variable and that can be molded as homogenous Poisson processes (HPP) with the respective failure rates. Repairable systems are often modelled as HPPs, where the inter-occurrence times of those failure events are independent with exponential behavior (i.e. constant system failure rates). One should note that system maintenance with “perfect repair” or replacement “as good as new” is assumed under HPPs (i.e. a renewal process). However, a constant failure rate cannot capture the system reliability throughout its life cycle, i.e. that behavior can be limited to a small part of the system life. Therefore, other system operational conditions such as mission reliability, reliability growth or deterioration, and maintenance policies cannot be included under constant failure rate models. System failures under “minimal repair” (i.e. as bad as old) are assumed in this study to develop a nonhomogeneous Poisson process (NHPP) that consists of a varying failure rate. The system failure rate in a NHPP model can have an increasing or decreasing trend and categorize as the system failure intensity of the selected system. Furthermore, this failure trend can be calculated by using the event data of the selected gas turbine engine under the Laplace trend test (LTT) and that is described in the following section.

2.3. Laplace trend test

A system failure rate with increasing (i.e. deteriorating the system reliability), constant (i.e. neither deteriorating nor improving the system reliability) or decreasing (i.e. improving the system reliability) trends can be captured by the LTT [35] and that for a selected system can be written as:

$$U_L = \frac{\sum_{i=1}^{N(T)} X_i}{N(T)} - \frac{T}{2} \Big/ T\sqrt{\frac{1}{12N(T)}} \tag{1}$$

when $U_L < 0$: has a decreasing failure trend (i.e. increasing system reliability), $U_L > 0$: has an increasing failure trend (i.e.

decreasing system reliability) and $U_L \approx 0$: has a neither increasing nor decreasing failure trend (i.e. neither decreasing nor increasing system reliability) in the system reliability. The test statistic is approximated to a standard normal distribution, therefore the significant level of the results can be observed from a standard normal table. e.g. for $|U_L| > 1.96$, the results satisfy the statistical significance level of 95%.

2.4. Failure rate

A NHPP as a failure trend model for a system is considered in this section. One should note that the time intervals between two failures are not IID in a NHPP, because the system age influences the system failure rate. The failure intensity of a system as a NHPP can be written as [36]:

$$\mu(t) = \lambda\beta t^{\beta-1} \tag{2}$$

when $\beta < 1$, $\mu(t)$ is decreasing (i.e. infant mortality phase), $\beta = 1$, $\mu(t)$ is a constant (i.e. useful life phase) and $\beta > 1$, $\mu(t)$ is increasing (i.e. wear-out phase) in the respective system. Furthermore, these conditions (i.e. $\beta < 1$, $\beta = 1$ and $\beta > 1$) also relate to the different sections of the famous "bath-tub curve" of a system life cycle [37].

2.5. Expected number of failures

The power-law mean value function (i.e. the expected number of failures,) for a NHPP with the failure intensity in (2) during the time period $(t_{i-1}\ \ t_i]$ can be written as ([38]–[39]):

$$\mathrm{E}[N(t_i - t_{i-1}) = n_i] = \lambda t_i^{\beta} - \lambda t_{i-1}^{\beta} \tag{3}$$

Hence, the probability of encountering n_i failures during the same time period can be written as:

$$\mathrm{P}[N(t_i - t_{i-1}) = n_i] = \frac{(\lambda t_i^{\beta} - \lambda t_{i-1}^{\beta})^{n_i} e^{-(\lambda t_i^{\beta} - \lambda t_{i-1}^{\beta})}}{n_i!} \tag{4}$$

Considering (3), the expected number of failures during the system age $(0\ \ T]$ can be simplified as:

$$\mathrm{E}[N(T)] = \lambda T^{\beta} \tag{5}$$

Furthermore, the mission reliability (i.e. the probability that the system functionalities satisfy the mission without any failures) for the system age $(t_{i-1}\ \ t_i]$ can be written as:

$$R(t) = e^{-\int_{t_{i-1}}^{t_i} \mu(t)dt} = e^{-(\lambda t_i^{\beta} - \lambda t_{i-1}^{\beta})}$$

2.6. Maximum likelihood estimation

The parameters of the NHPP model in (1) should be estimated to identify the failure intensity of a system. That can be done by considering an event data set (i.e. system failure events) of the system under the maximum likelihood estimation (MLE). One should note that the MLE has several optimal properties with respect to the parameter estimation process [40]. Considering (4), the likelihood function [41] can be written as:

$$L(\lambda,\beta) = \prod_{i=1}^{\bar{n}} \mathrm{P}(N(t_i - t_{i-1}) = n_i) = e^{-\lambda T^{\beta}} \prod_{i=1}^{\bar{n}} \frac{(\lambda t_i^{\beta} - \lambda t_{i-1}^{\beta})^{n_i}}{n_i!} \tag{7}$$

Considering (7), the log likelihood function can be written as:

$$\log L(\lambda,\beta) = -\lambda T^{\beta} + \sum_{i=1}^{\bar{n}} n_i(\log\lambda + \log(t_i^{\beta} - t_{i-1}^{\beta})) - \log n_i! \tag{8}$$

The partial derivatives of (8) with respect to both parameters, λ and β, are considered for the MLE and resulted in:

$$\frac{\partial}{\partial\lambda}\log L(\lambda,\beta) = -T^{\beta} + \frac{1}{\lambda}\sum_{i=0}^{\bar{n}} n_i = 0$$

$$\frac{\partial}{\partial\beta}\log L(\lambda,\beta) = -\lambda T^{\beta}\log T + \sum_{i=1}^{\bar{n}} n_i \frac{(t_i^{\beta}\log t_i - t_{i-1}^{\beta}\log t_{i-1})}{(t_i^{\beta} - t_{i-1}^{\beta})} = 0 \tag{9}$$

Hence, the MLE values of λ and β should satisfy the following conditions:

$$\widehat{\lambda} = \frac{\sum_{i=1}^{\bar{n}} n_i}{T^{\widehat{\beta}}} = \frac{N(T)}{T^{\widehat{\beta}}}$$

$$-\widehat{\lambda} T^{\widehat{\beta}} \log T + \sum_{i=1}^{\bar{n}} n_i \frac{(t_i^{\widehat{\beta}} \log t_i - t_{i-1}^{\widehat{\beta}} \log t_{i-1})}{(t_i^{\widehat{\beta}} - t_{i-1}^{\widehat{\beta}})} = 0 \tag{10}$$

One should note that the solution in (10) can be calculated iteratively and that has a unique solution for the parameters of λ and β. This solution can be derived for time or failure truncated situations of a system. A situation with the observations that are truncated after a prefixed time interval for a respective number of failures (i.e. the number of failures is a random variable) is considered as time truncated. A situation with the observations truncated after a prefixed number of failures of the respective time interval (i.e. the time interval is a random variable) is considered as failure truncated. However, a time truncated situation for the time period (T_S T_E] (i.e. the total operational period) of a system is considered in this study. Hence, (10) can be presented in a closed form [42]:

$$\widehat{\lambda} = \frac{N(T_E - T_S)}{T_E^{\widehat{\beta}} - T_S^{\widehat{\beta}}}$$

$$\widehat{\beta} = \frac{N(T_E - T_S)}{\widehat{\lambda}\,(T_E^{\widehat{\beta}} \log T_E - T_S^{\widehat{\beta}} \log T_S) - \left[\sum_{i=1}^{N(T_E - T_S)} \log X_i\right]} \tag{11}$$

One should note that that (11) can also be simplified [43] for the system age, (0 T], as:

$$\widehat{\lambda} = \frac{N(T)}{T^{\beta}}$$

$$\widehat{\beta} = \frac{N(T)}{\sum_{i=1}^{N(T)} \log\left(\frac{T}{X_i}\right)} \tag{12}$$

2.7. Unbiased estimate

Furthermore, the unbiased estimator for β in (12) for the system age, (0 T] can be written as [38]:

$$\overline{\beta} = \frac{N(T) - 1}{N(T)} \widehat{\beta} \tag{13}$$

One should note that $\widehat{\lambda}$ is the unbiased estimator for the parameter, λ in (12).

2.8. Confidence bounds and hypothesis testing

The confidence bounds for the true value of β under the MLE can be derived by considering a Chi-square distribution with $2N(T)$ degrees of freedom [36,38]:

$$\chi^2_{MLE} = \frac{2N(T)\beta}{\widehat{\beta}} \tag{14}$$

where $N(T)$ is moderate with statistics $\omega = \sqrt{N(T)}\left(\frac{\beta}{\widehat{\beta}} - 1\right)$. Therefore, the approximate confidence bounds (i.e. the $(1-\alpha)\cdot 100$ percent lower and upper confidence bounds) for β can be written as:

$$[\beta_{LB} \quad \beta_{UB}] \equiv \left[\widehat{\beta}\left(1 - \frac{P_\pi}{\sqrt{N(T)}}\right) \quad \widehat{\beta}\left(1 + \frac{P_\pi}{\sqrt{N(T)}}\right)\right] \tag{15}$$

Furthermore, the respective lower and upper confidence bounds for λ can be written as:

$$[\lambda_{LB}(\beta_{UB}) \quad \lambda_{UB}(\beta_{LB})] \equiv \left[\frac{\chi^2\left(\frac{\gamma}{2}, 2N(T)\right)}{2T^{\beta_{UB}}} \quad \frac{\chi^2\left(1 - \frac{\gamma}{2}, 2N(T) + 2\right)}{2T^{\beta_{LB}}}\right] \tag{16}$$

One should note that (15) and (16) are categorized as the conservative simultaneous confidence bounds (i.e. the $(1-\alpha)(1-\gamma)\cdot 100$ percent lower and upper confidence bounds) for λ and β.

2.9. Goodness-of-fit test

The model parameters in (11) should be calculated to identify the failure intensity of a system, then the model in (2) that predicts

estimated system failures should be compared with actual system failures to evaluate system-model uncertainties. That can be done by two statistical tests (i.e. goodness-of-fit tests): Cramer-Von Mises goodness-of-fit test and Chi-square test.

2.9.1. Cramer-Von Mises goodness of fit test

The Cramer-Von Mises goodness-of-fit test can be written as [44]:

$$C_M^2 = \frac{1}{12N(T)} + \sum_{i=1}^{N(T)} \left(\left(\frac{X_i}{T} \right)^{\overline{\beta}} - \frac{2i-1}{2N(T)} \right)^2 \tag{17}$$

Cramer-Von Mises goodness statistics can be used to test various hypothesis, where the proposed NHPP model capabilities with the estimated parameters to capture the actual system failure events can be evaluated. That is done by introducing two hypothesis under the Cramer-Von Mises goodness-of-fit test: hypothesis H_1: system failures with a constant failure rate (i.e. $\overline{\beta} = 1$,) and hypothesis H_2: system failures with a NHPP with the proposed intensity function (i.e. $\overline{\beta}$ is unspecified). The test outcome can be summarized as: if ${C_M}^2$ is less than the selected critical value, then hypothesis H_1 is rejected and hypothesis H_2 is accepted at the respective significant level. Therefore, the proposed failure intensity model in (2) with the estimated parameters of λ and β can be accepted [38]. Otherwise the test results are inconclusive.

2.9.2. Chi-square test

The Cramer-Von Mises goodness-of-fit test requires that the initial time should be 0 (Hrs). Therefore, that test cannot be implemented on a system with various erroneous data conditions (i.e. missing data, varying failure intensity, and unknown system age situations) [45]. The Chi-square test with $N_d - 2$ degrees of freedom is proposed to overcome such situations (i.e. the events data with several discrete data intervals) and that can be written as [36]:

$$\chi^2 = \sum_{i=1}^{N_d} (N_i - \widehat{\theta}_i)^2 / \widehat{\theta}_i \tag{18}$$

2.10. Erroneous data conditions

It is expected that the proposed failure intensity model of a selected gas turbine engine may not satisfy the required goodness-of-fit test in some situations due to various erroneous data intervals in CM data [46]. e.g. a large number of failures can be reported within a small-time interval due to several startup failures in a gas turbine engine. Therefore, the following steps are proposed to identify and isolate such erroneous data intervals in CM data.

- Firstly, the event data (i.e. CM data) of a selected gas turbine engine are used to derive the proposed failure intensity model in (12) and categorized as “single interval data analysis”.
- Then, the model is tested with the goodness-of-fit test in (17) with the actual failure events.
- If the proposed model fails to satisfy the goodness-of-fit test, then the erroneous data intervals from the recorded events are identified and isolated, i.e. the event data interval separates into sub data intervals.
- Then, several failure intensity models are derived for each sub data interval and categorized as “multi-interval data analysis”.
- Finally, each new model is also tested with the goodness-of-fit test in (17) & (18) with the actual failure events.

Furthermore, this process should continue until the proposed failure intensity models satisfy the goodness-of-fit tests within the required confidence interval.

2.11. Mean time between failures

The proposed failure intensity model (i.e. that satisfies the goodness-of-fit test within the required confidence interval) in (2) can be used to calculate the instantaneous mean time between failures (MTBF) [47] for the same system and that can be written as [48]:

$$\widehat{M}(t) = (\widehat{\mu}(t))^{-1} = (\widehat{\lambda}\widehat{\beta}t^{\widehat{\beta}-1})^{-1} \tag{19}$$

Furthermore, the confidence interval for $\widehat{M}(t)$ provides the measure of uncertainty around the calculated value in (19). Hence, the two sided $(1-\alpha)\cdot 100$ percent confidence intervals (i.e. the lower and upper confidence bounds) can be written as:

$$\Pi_1 \widehat{M}(t) \le \widehat{M}(t) \le \Pi_2 \widehat{M}(t) \tag{20}$$

where Π_1 and Π_2 can be obtained from the available data tables in [44].

3. Parameter estimation

The proposed failure intensity model of a selected gas turbine engine is derived in this section by considering its CM data. This data set consists of various system shutdown and failure events of the gas turbine engine and those events are visualized in a more detailed view in the following figures.

3.1. Failure events

The system shutdown and failure periods, i.e. the event data, for the selected gas turbine engine in the last 4 year period are presented in Fig. 3. Various failure events are recorded with respect to subsystem and component faults in the gas turbine engine. A summary of those events (i.e. shutdown and failure events) and their respective event codes are presented in Table 1. One should note that 34 event codes with respect to gas turbine engines are considered in this study. Furthermore, a summary of the total shutdown and failure events that are obtained from the same data set of the gas turbine engine for the same period is presented in Table 2. This event data set consists of 34,708 (Hrs) and that period is divided into 10 operational intervals (i.e. each 3500 (Hrs) data interval) in the figure to improve the information visibility. The shutdown and failure periods are denoted as blue and red blocks, respectively in the same figure. Then, the cumulative non-shutdown period for the gas turbine engine is derived from the same data set, where the shutdown periods are removed by connecting the non-shutdown periods. A connection point of two non-shutdown periods is considered as an event separator, i.e. combined non-shutdown period (CNSP) separators (see Fig. 4), and such event separators are introduced to track continues non-shutdown periods. Furthermore, the respective failure periods are also adjusted accordance with the removed shutdown periods. Therefore, the combined non-shutdown period has reduced to 23,649 (Hrs) from the total period of 34,708 (Hrs). The CNSP, respective event separators, and adjusted failure periods are also presented in Fig. 4. One should note that the failure periods of the gas turbine engine are compressed as the respective failure events, i.e. CNSP separators. This step assumes that the system failure events of the gas turbine engine are recovered by a same number of repairs with negligible maintenance periods. The total operational period (i.e. the system age) of the gas turbine engine is derived by this step and approximately reduced from 23,649 (Hrs) to 22,596 (Hrs). The system operational period (i.e. calculated operational hours (COHs)), COH event separators, and failure events are presented in Fig. 5.

It is observed that an internal data processing unit in the gas turbine engine also records its operational hours. Those events are categorized as the machine recorded operational hours (MROHs) and presented with the MROH event separators in the same figure. It is expected that the MROHs should coincide with the COHs because the both data sets represent the same shutdown and failure events of the gas turbine engine. One should note that this approach considers the same failure events of the gas turbine engine by analyzing two data sets (i.e. COHs from an external data recording system and MROHs from internal data recording system). Therefore, the accuracy of the respective failure events and data recording systems can be verified. However, the results (see Fig. 5) show the MROHs have shorter periods with respect to the COHs of the gas turbine engine. Therefore, the reasons for such time variations are further investigated. It is noted that the system start-up and shutdown hours, i.e. time periods, have not been properly recorded under the MROHs, because the internal data processing unit may not operate properly during the start-up and shutdown periods. Therefore, the MROHs consist of shorter periods than the COHs and that have introduced the time variations between the COHs and MROHs. However, the number of failures events coincides in both systems, i.e. COHs and MROHs, therefore that is a good indication that the failure events are occurred in the respective order. Furthermore, it is also concluded that the same gas turbine engine has been used throughout the CM period (i.e. the machine has not been replaced with another machine) by considering the continuous MROH values.

The number of failures of the gas turbine engine at each short-time interval with respect to the system age (i.e. the operational

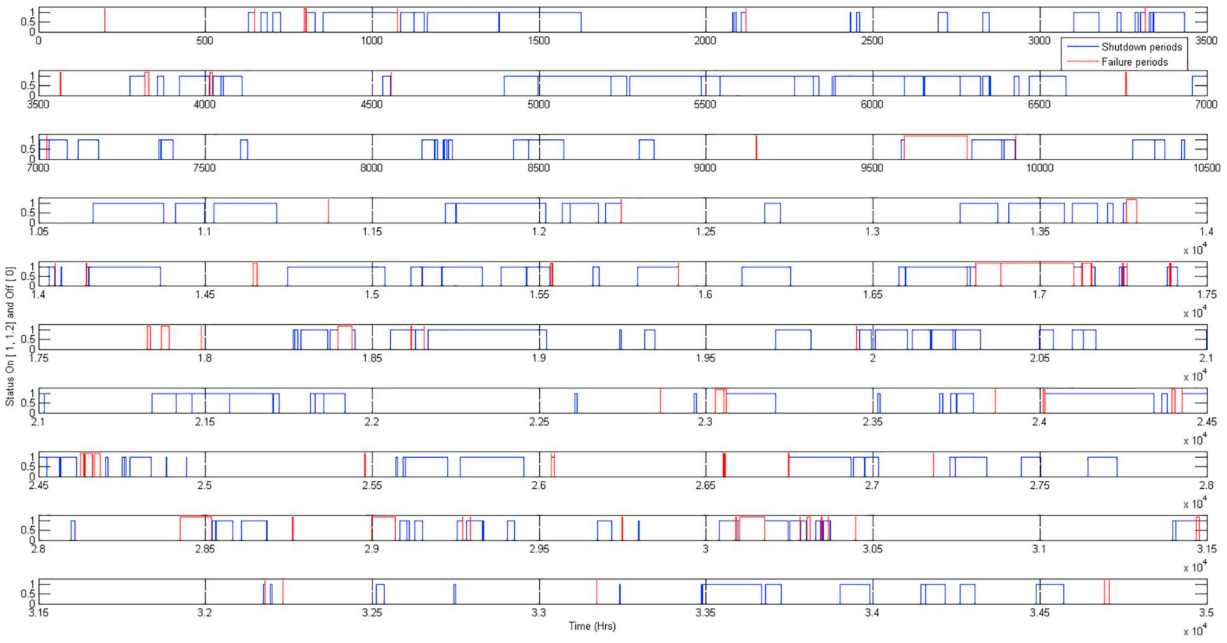

Fig. 3. Shutdown and Failure periods for the selected gas turbine engine.

Table 1
Event descriptions and codes (2008–2012, Petrobras, Rio De Janeiro, Brazil).

No	Event description	Fault code
1	Changes in the machine status	79.000
2	Normal Shutdown	79.001
3	Failsafe Shutdown	79.004
4	Over-fuel to ignition failure shutdown	79.006
5	Ignition failure shutdown	79.008
6	Low pressure compressor: software over-speed shutdown	79.010
7	Start system speed: crash re-engagement shutdown	79.012
8	Gas upstream pressure fault shutdown	79.027
9	Gas downstream pressure fault shutdown	79.028
10	Liquid upstream pressure fault shutdown	79.042
11	Variable inlet guide vane in linear variable differential transformer: position error shutdown	79.046
12	Gas generator module temperature high shutdown	79.064
13	Gas generator exhaust average temperature high shutdown	79.065
14	High speed shaft of gearbox: drive end vibration high shutdown	79.068
15	Low speed shaft of gearbox: non drive end vibration high shutdown	79.075
16	Generator non-drive end vibration high shutdown	79.081
17	Gas generator starter differential crash speed shutdown	79.091
18	High compressor of gas generator: speed low shutdown	79.096
19	Low compressor of gas generator: speed low shutdown	79.097
20	Main lube oil rundown tank fill time-out	79.098
21	Gas generator light-up verification timeout	79.099
22	Gas generator Acceleration time-out	79.100
23	Common vibration shutdown	79.111
24	Fire and gas emergency general alarm	79.113
25	Common shutdown	79.116
26	Excitation trip	79.117
27	Generator protection shutdown	79.118
28	Emergency shutdown: pushbutton 2	79.120
29	Waste heat recovery unit inlet/bypass damper linkage failure	79.123
30	Hydraulic start control panel shut-down	79.126
31	Emergency shutdown: pushbutton on main generator control panel	79.145
32	Emergency shutdown: the whole platform	79.146
33	Liquid fuel supply pressure low shutdown	79.147
34	Generator set supply breaker tripped by protect	79.148

Table 2
Event summary (2008–2012, Petrobras, Rio De Janeiro, Brazil).

No	Event type	Number of occurrences
1	Total events	331
2	Shutdown Events	221
3	System Failures	110

period) is calculated by considering the COHs and presented in plot (a) of Fig. 6. The number of failure events in this time period is calculated as 110 (see Table 2) and the respective periods of the MROHs and COHs with respect to each failure event are presented in plot (b) of Fig. 6. Furthermore, the respective errors between the MROHs and COHs are presented in plot (c) of Fig. 6. In general, the error values between the MROHs and COHs are increasing along the system age due to the internal data processing unit failures as discussed previously. One should note that these errors have increased to a larger value and then decreased to a much lower value in some situation. That outcome shows that the internal data processing unit introduces additional time-delays on recording the MROHs.

A failure transition diagram derived by the COHs for the same system events of the gas turbine engine is presented in in Fig. 7. This diagram consists the conditional probability (i.e. the number along the state transition arrow) of the system transition from one fault state to another fault state. One should note that the criticality of each system fault is presented by various colors (i.e. red: the most critical and blue: the least critical) and radii, where the respective event codes (i.e. the last three numbers of the events from 79.000 to 79.126) are also denoted (see Table 1). The conditional probability values are estimated by considering the number of failure transitions of the gas turbine engine from one fault state to another fault state. Therefore, each fault state consists of several transition situations to its own state and other fault states. The number of failure transitions to its own state and other fault states is divided by the total number to failure transitions from each fault state to calculate the respective conditional probability values. Therefore, this diagram shows the respective relationships among various system faults in the gas turbine engine. e.g. how frequent each system fault can occur and the possible future faults from the present system fault. The same information can be used to derive appropriate maintenance policies (i.e. to avoid criticality system faults) in offshore power plants and that is beyond the scope of this study.

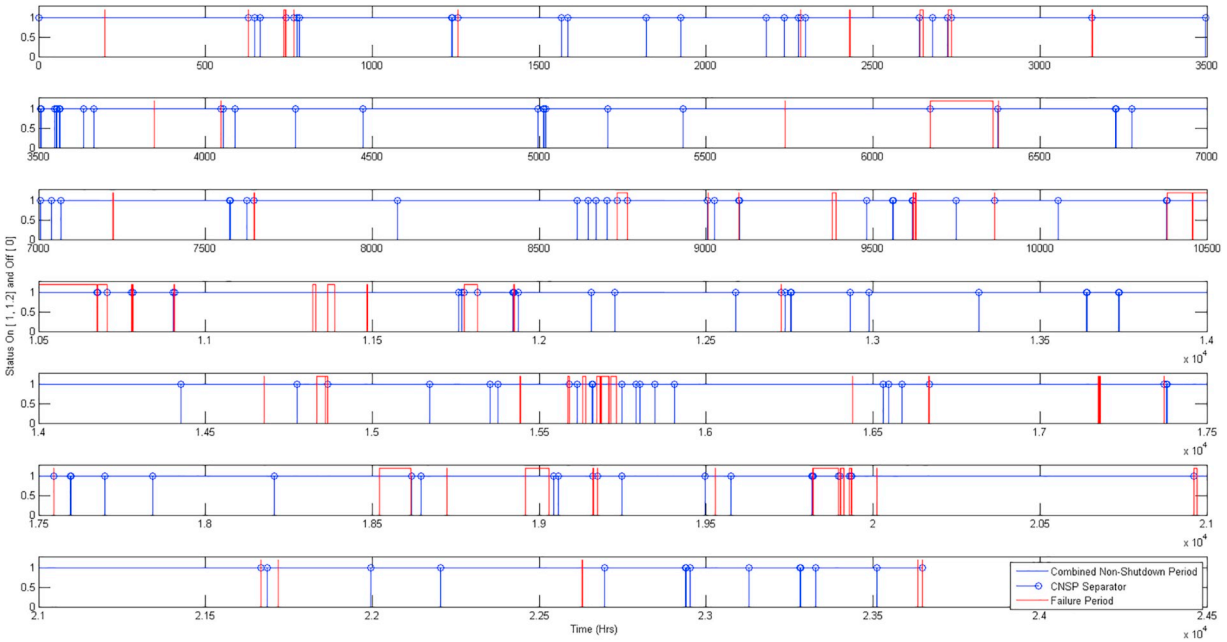

Fig. 4. Non-Shutdown and Failure periods for the selected gas turbine engine.

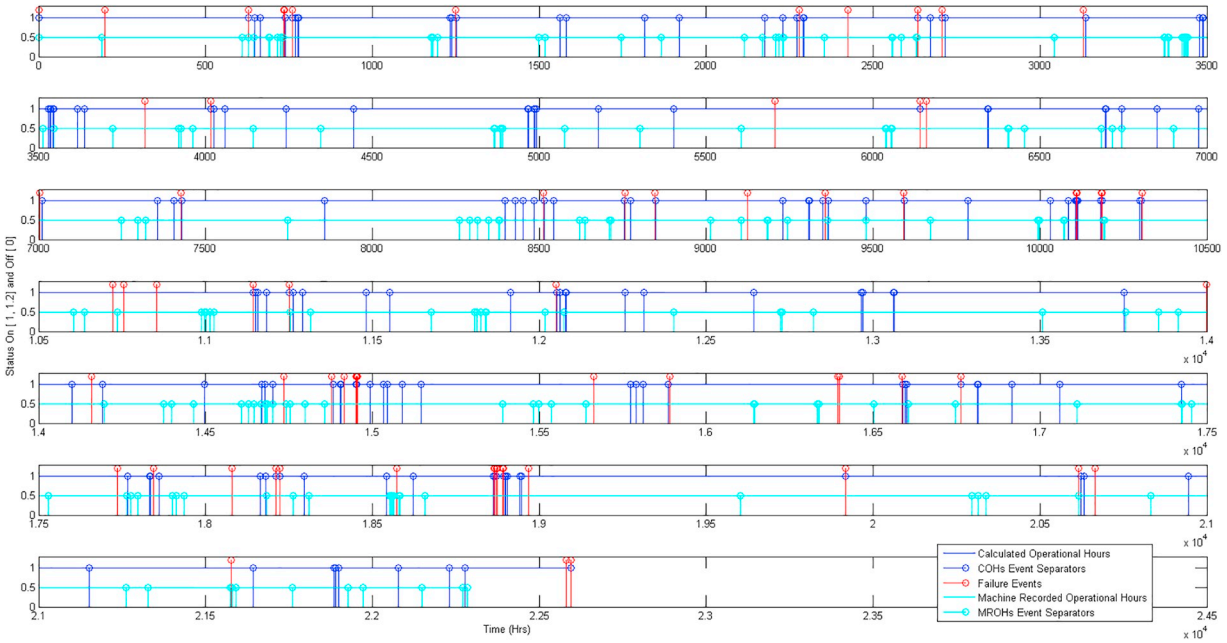

Fig. 5. Operational period and Failure events for the selected gas turbine engine.

3.2. Single interval data analysis

Single interval data analysis is considered in this section. The LTT in (1) is used to evaluate the system failure trend in the gas turbine engine by considering the COHs and the outcome can be written as:

$$U_L = 1.1894 \tag{21}$$

Therefore, this gas turbine engine has a slightly increasing failure trend (i.e. decreasing reliability is concluded by (21)) with the respective statistical significance of 88%. The proposed NHPP in (2) for modeling the system failure intensity of the gas turbine engine is considered with a time truncated situation (i.e. the system age as $T = 22596$ (Hrs)). The model parameters in (2) are derived by considering the COHs with (12) and the outcome can be written as:

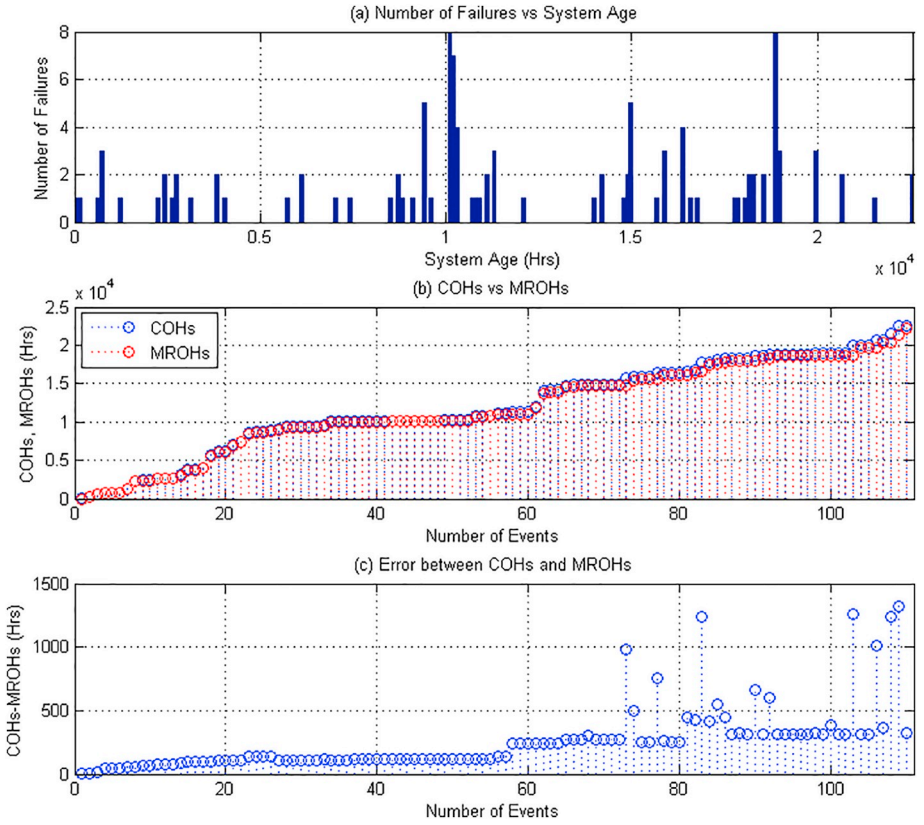

Fig. 6. COHs and MROHs data for a selected gas turbine engine.

$$\widehat{\lambda} = 0.0028$$

$$\widehat{\beta} = 1.0542 \tag{22}$$

One should note that this gas turbine engine is in a slightly wear-out phase. Hence, the unbiased estimate of βcan be calculated by (13) and the outcome can be written as:

$$\overline{\beta} = 1.0447 \tag{23}$$

Furthermore, the approximate confidence bounds for β with the lower and upper confidence bounds can be calculated by (15) and the outcome can be written as:

$$\beta_{LB} = 0.9254$$

$$\beta_{UB} = 1.1831 \tag{24}$$

Similarly, the lower and upper confidence bounds for λ can be calculated by (16) and the outcome can be written as:

$$\lambda_{LB} = 6.5879{\cdot}10^{-4}$$

$$\lambda_{UB} = 0.0121 \tag{25}$$

One should note that the 81% conservative simultaneous confidence bounds for λ and β are presented in (24) and (25) with $\alpha = .1$ and $\gamma = .1$. These model parameters are used to derive the following figures. The failure intensity for the gas turbine engine in (2) with the parameter values in (22) with respect to the system age is presented in plot (a) of Fig. 8. Furthermore, the respective mission reliability in (12) for a 15 day (i.e. 360 (Hrs)) time interval is presented in plot (b) of Fig. 8. One should note that the mission reliability is decreasing with respect to the system age in this situation. The expected number of failures with in the next 15 day (i.e. 360 (Hrs)) time period at the system age, 22,596 (Hrs), is calculated by (5) and resulted in 1.85 failure events per 15 days (i.e. MTBF is approximately 194.85 (Hrs)). Therefore, it is concluded that approximately 2 system failures in average in every 16 days (i.e. operational days) can be encountered by this gas turbine engine under the present operational conditions. The instantaneous MTBF in (19) for the same gas turbine engine is presented in plot (c) of Fig. 8. One should note that the MTBF value has converged approximately to 194.85 (Hrs) (i.e. 8.12 (days).) at the respective system age. The estimated lower and upper bounds for the MTBF with two-sided 90% confidence intervals are calculated by (20) and the outcome can be written as:

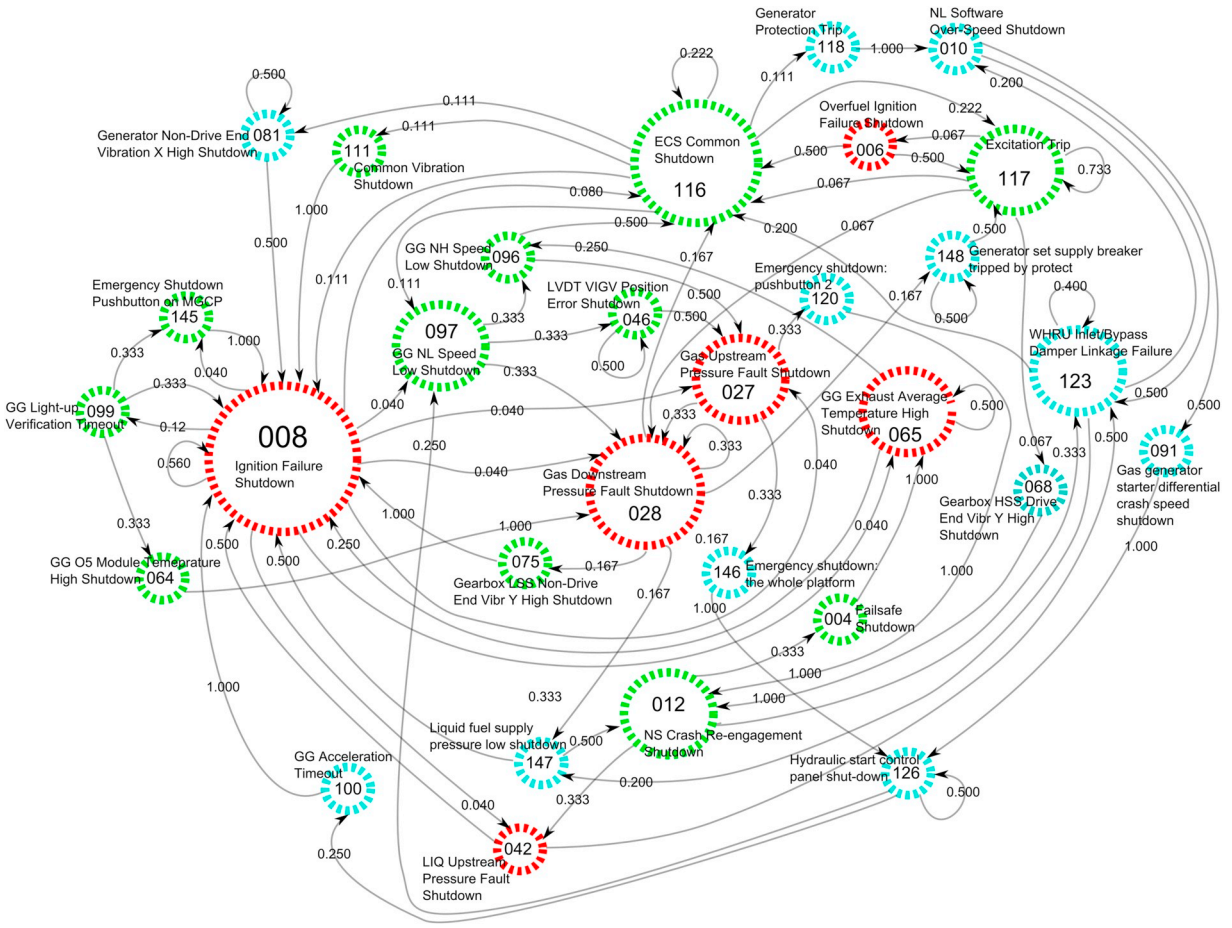

Fig. 7. Failure Transition Diagram for the selected gas turbine engine.

$$156.27\,(\text{Hrs}) \leq \widehat{M}\,(T = 22596(Hrs)) \leq 246.48\,(\text{Hrs}) \tag{26}$$

where the respective table values can be extrapolated as $\Pi_1 = 0.802$ and $\Pi_2 = 1.265$. Considering these calculations, it is concluded that the gas turbine engine can encounter one system failure from 6.51 (days) (156.27 (Hrs)) to 10.27 (days) (246.46 (Hrs)). The actual and predicted (i.e. estimated) failures of the gas turbine engine with respect to its system age are presented in plot (a) of Fig. 9. One should note that the predicted failures are derived from the failure intensity model in (2) with the respective parameters in (22). Furthermore, the actual and predicted (i.e. estimated) average failure rates for the gas turbine engine under 10 discrete data intervals are presented in plot (b) of Fig. 9. It is noted that the actual average failure rates have relatively higher values with compared to the actual estimated failure rates in two situations. Both plots show an increasing failure trend with respect to the system age and some deviations of the actual failures with respect to the predicted failures for the gas turbine engine can also be noted.

As the final step of this data analysis, a goodness-of-fit test is conducted with respect to the actual and predicted system failure events. The Cramer-Von Mises goodness-of-fit in (17) for the failure intensity model in (2) with the estimated parameters in (22) is conducted to evaluate the system-model uncertainties in relation to failure events of the gas turbine engine. The requirements for the Cramer-Von Mises goodness-of-fit can be summarized as [43]: ${C_M}^2 < {C_T}^2$, then the model is accepted for the same significant level, where $N = 110$, $\alpha = 0.01$ and ${C_T}^2 \approx 0.34$. The Cramer-Von Mises goodness-of-fit test for this model is calculated by (17) with the outcome of ${C_M}^2 = 0.4315$. Therefore, the model in (2) with the respective parameter values in (22) has failed to satisfy the Cramer-Von Mises goodness-of-fit with in the respective significant level because of $C_M^2 > {C_T}^2$. Considerable deviations from the actual system failures with respect to the predicted system failures in the gas turbine engine are observed in some situations and that can be confirmed by these test results.

However, several important observations are also noted during this data analysis. Firstly, $\widehat{\beta}$ can be approximated to 1, therefore the LTT supports neither increasing nor decreasing failure trends with the respective statistical significance. Secondly, a large number of failures are observed in two time intervals, i.e. approximately around 10,000 (Hrs) and 18,923 (Hrs) of the system age (see plot (b) Fig. 9), and that may relate to repeated start-up and shutdown failures or component failures in the gas turbine engine. Thirdly, this gas turbine engine has gone through various maintenance policies during its life time. These policy variations can also influence on the system failure intensity, therefore the gas turbine engine can have several failure intensity levels in different sectors of its system

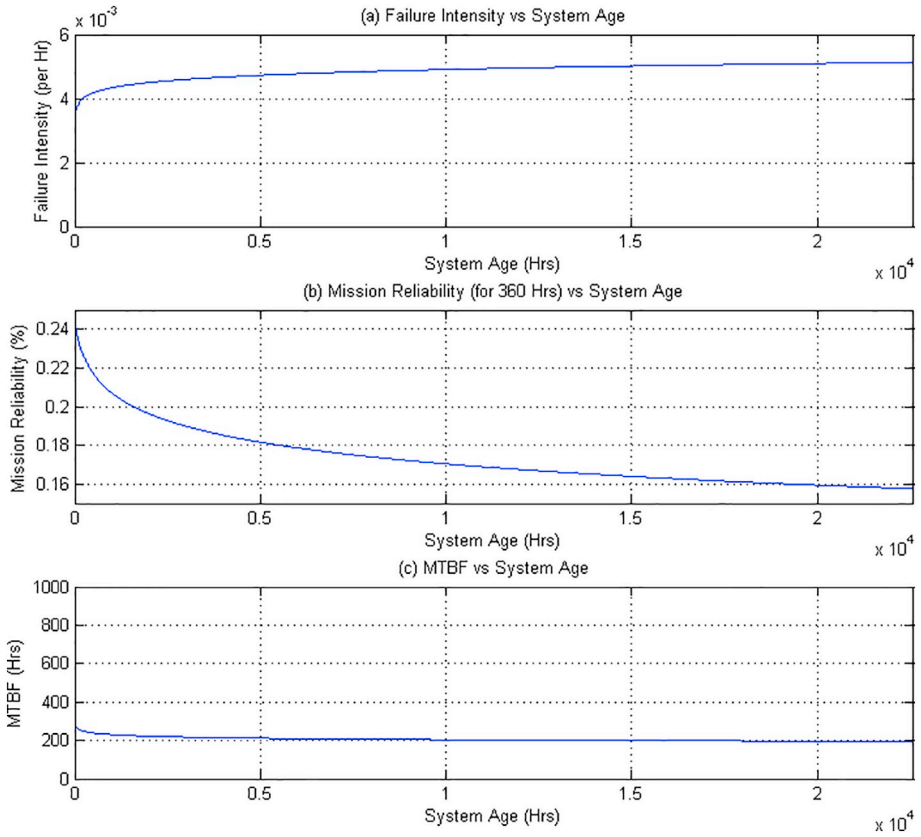

Fig. 8. Proposed model behaviour for the selected gas turbine engine.

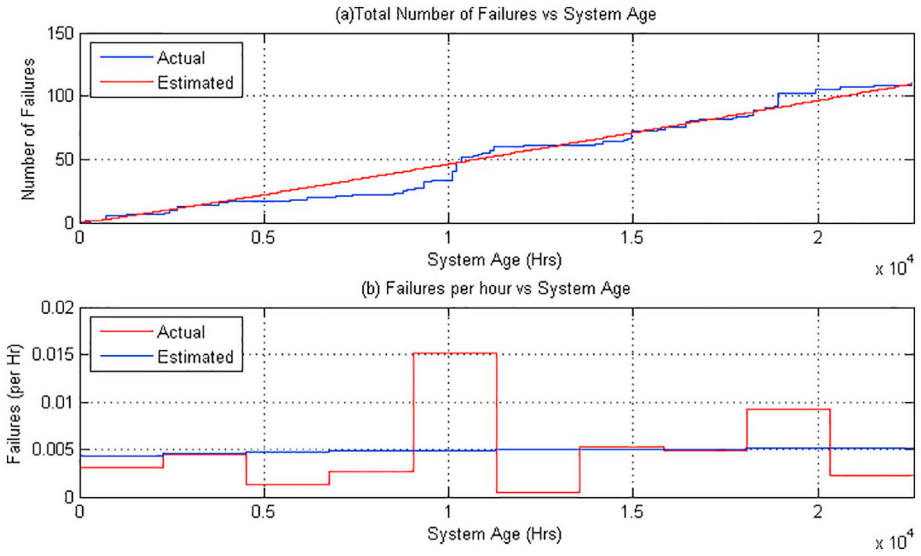

Fig. 9. System and model comparison for the selected gas turbine engine.

age, rather than a single failure intensity model. Hence, one or more such reasons may have introduced such erroneous data conditions into the COHs. That have eventually influenced on the proposed failure intensity model of the gas turbine engine, where a considerable deviation of the actual system failures with respect to the predicted system failures are observed.

As the next step of this analysis, the same gas turbine engine with several failure intensity levels in different sectors of its system age is considered to overcome the goodness-of-fit test failure. Furthermore, the respective sectors of the system age of this gas turbine engine are analyzed. A detailed view of the failure events (with error codes) of the gas turbine engine is presented in plots (a) of

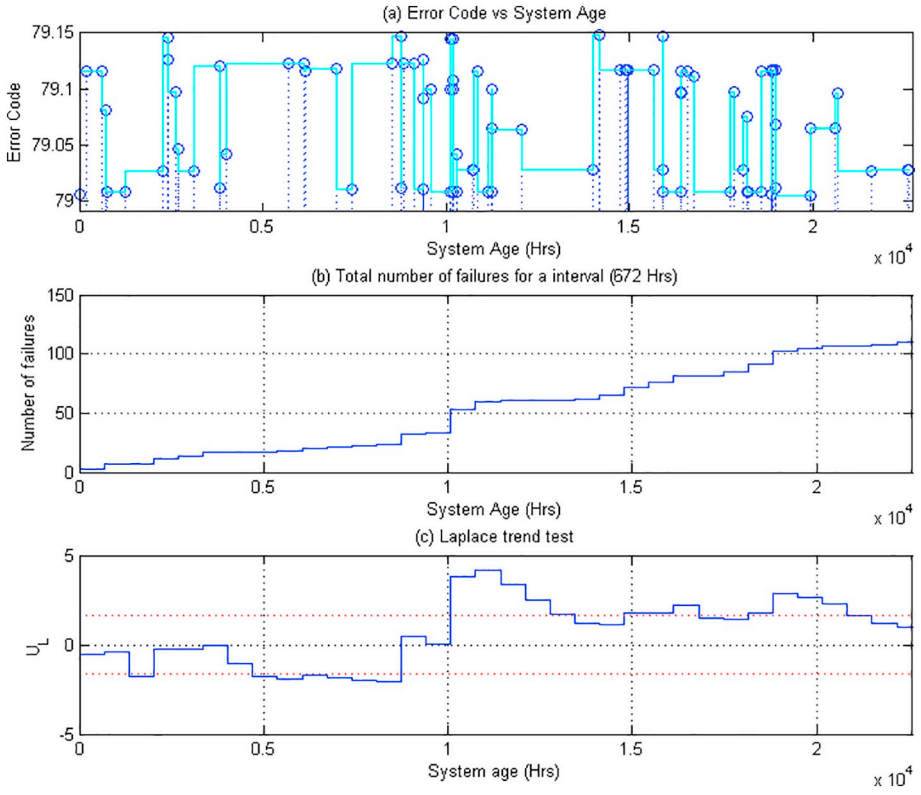

Fig. 10:. Failure events for the selected gas turbine engine.

Fig. 10. The total number of the failure events with respect to the system age is presented in plot (b) of the same figure and that has derived by considering a data interval of 672 (Hrs). Two large increments in the actual system failures of the gas turbine engine can be observed approximately around 10,000 (Hrs) and 18,923 (Hrs) of the system life (see plot (b) Fig. 9) as discussed previously. Therefore, such situations are considered as erroneous data conditions and that are isolated from the data analysis, i.e. those situations have separated the system life of the gas turbine engine into several sectors. The LTT is used again to analyze these life sectors of the gas turbine engine.

3.3. Multi-interval data analysis

The LTT with 672 (Hrs) time intervals for the COHs is analyzed in this section by separating the system life of the gas turbine engine into several sectors. It is assumed that that each data interval starts from 0 (Hrs) continue to 672. i (Hrs) of the system age, where $i = 1, 2, \ldots 65$ (i.e. the data interval length is increased continuously by adding each sector). One should note that this approach can be used to observe the variations in the failure trends in the gas turbine engine throughout its system life and the test results are presented in plot (c) of Fig. 10. The significance level of 0.10, the critical value of 1.645 (i.e. the standard normal table), is also presented in dotted lines in the same figure. The results show $U_L < 0$until the system age approximately 10,000 (Hrs) and $U_L > 0$ for the rest of the system age. Therefore, it is concluded that the gas turbine engine has an increasing failure trend until the system age approximately 10,000 (Hrs) and a decreasing failure trend for the rest of the system age (i.e. two failure rates). Therefore, the COHs are divided into two data intervals (i.e. the system life of the gas turbine engine into several sectors as data interval I and II), where the respective failure intensity models for the gas turbine engine are calculated.

3.3.1. Data interval I

The first data interval is considered as $(0 \quad T_{S1}(\approx 10000.\ (Hrs))]$ and the respective parameters for the failure intensity model in (2) are calculated by (12) and the outcome can be written as:

$$\widehat{\lambda} = 0.0298$$

$$\widehat{\beta} = 0.7612 \tag{27}$$

The total number of failure events in this data interval is calculated as 33 and (27) is denoted as Model 1. One should note that $\widehat{\beta} < 1$ for this data interval, therefore some improvements in the system reliability of the gas turbine engine due to maintenance actions are concluded. Furthermore, the Cramer-Von Mises goodness-of-fit test in (23) for this model is calculated for $N_1 = 33$ and the

outcome can be written as: $C_M{}^2 = 0.2783$. Hence, hypothesis H_1 is rejected because $C_T^2(\approx 0.337) > C_M{}^2$ for the significant level of $\alpha = 0.01$, where the failure intensity model in (2) with the respective parameters in (27) is accepted for the respective data interval. The first data interval (int. 1) with the actual (Actual) and predicted (Model 1) system failures is presented in plot (a) of Fig. 11. Furthermore, the data interval, $(T_{S1}(\approx 10000\,(Hrs))\ \ T_{S2}(\approx 10307.5\,(Hrs))]$, is considered as an erroneous region, where 19 system failures have occurred. A zoomed view of this erroneous data region is presented in plot (b) of the same figure.

3.3.2. Data interval II

The second data interval is considered as $(T_{S2}(\approx 10307.5\,(Hrs))\ \ T\,(\approx 22596\,(Hrs)]$ and the respective parameters for the failure intensity model in (2) are calculated by (11) and the outcome can be written as:

$$\widehat{\lambda} = .000182$$

$$\widehat{\beta} = 1.308 \tag{28}$$

The total number of failure events in this data interval is calculated as 70 and (28) is denoted as Model 2. One should note that $\widehat{\beta} > 1$ for this data interval, therefore some degradations in the system reliability of the gas turbine engine due to aging effects and/or poor maintenance actions can be concluded. The second data interval (int. 2) with the actual (Actual) and predicted (Model 2) system failures is presented in plot (a) of Fig. 11. Furthermore, the respective failure intensity functions (Model 1 & 2) for the gas turbine engine with respect to its system age for both time intervals (i.e. int. 1 & int. 2) are presented in plot (a) of Fig. 12. The respective mission reliability plots for a 15 day (i.e. 360 (Hrs)) interval under both time intervals are also presented is presented in plot (b) of the same figure. One should note that the mission reliability has an increasing trend in data interval I and a decreasing trend in data interval II. Therefore, a considerable reliability reduction in the mission reliability of this gas turbine engine can be noted after the first 10,000 (Hrs) of the system age despite the maintenance actions. The expected number of failure within the next 15 days (i.e. 360 (Hrs)) at the end of operational hours of 22,596 (Hrs) is calculated as 1.89 failures per 15 days (i.e. 360 (Hrs)). One should note that this expected number of failures of the gas turbine engine is slightly higher than the previously calculated value (i.e. approximated to 1.85 failure events per 15 days). However, the previous conclusion, approximately 2 system failures per every 16 days (i.e. operational days), can still be held under these calculations. The instantaneous MTBF for the gas turbine engine in both time intervals (i.e. int. 1 & int. 2) is presented in plot (c) of Fig. 12.

One should note that the MTBF value is reduced to 191.15 (Hrs) (i.e. 7.97 (days)) at the end of the 2-nd time interval, therefore the gas turbine may have a slightly higher failure rate than the previously calculated value (i.e. approximated to 8.12 (days)). The estimated lower and upper bound for the MTBF with 90% confidence interval can be calculated by (20) and the outcome can be

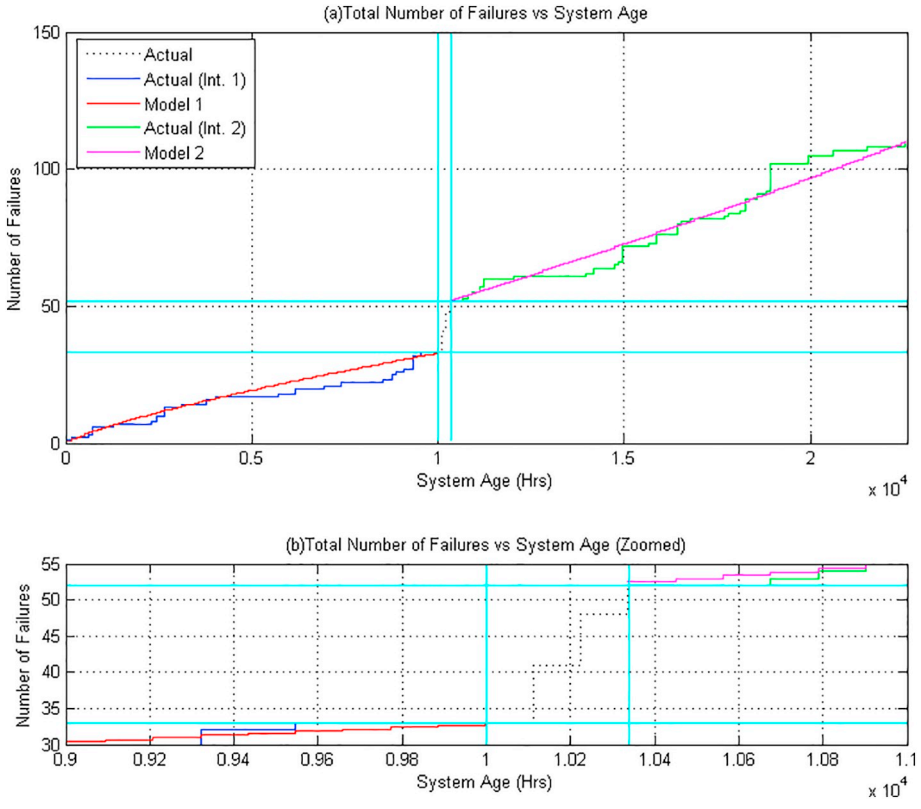

Fig. 11:. System-model comparison for the selected gas turbine engine.

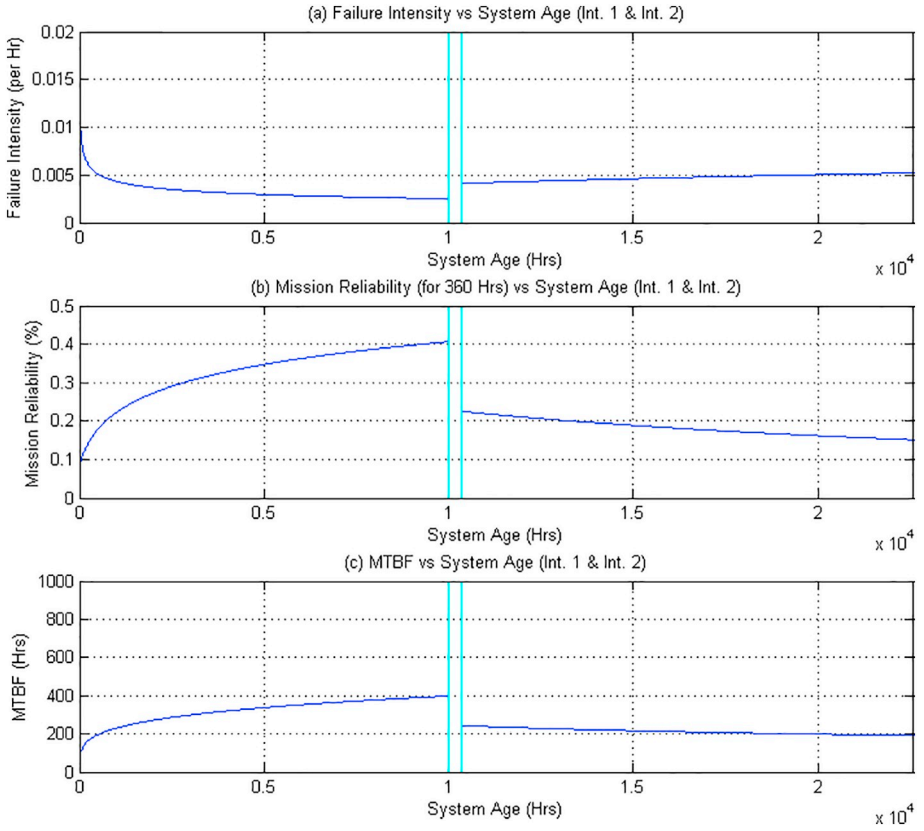

Fig. 12:. Proposed new model behaviour for the selected gas turbine engine.

written as [43]:

$$153.30\,(\text{Hrs}) \le \widehat{M}\,(T = 22596(Hrs)) \le 241.80\,(\text{Hrs}) \tag{37}$$

Therefore, the gas turbine engine can approximately encounter one system failure during 6.39 (days) to 10.08 (days) during the 2-nd time interval. The Cramer-Von Mises goodness-of-fit test cannot be implemented on data interval II as previously discussed. Therefore, the Chi-square test is used with $N_d = 8$ (i.e. the total number of data intervals), and the results are summarized in Fig. 13. The actual and predicted failures of the gas turbine engine are presented in plots (a) and (b) of Fig. 13, respectively. Furthermore, the i-th data interval chi-square value, $\chi_i^2 (=(N_i - \widehat{\theta}_i)^2/\widehat{\theta}_i)$, is presented in plot (c) of Fig. 13, where $i = 1, 2, \ldots, 8$. Finally, the summation of the chi-square values up to the i-th data interval, $\sum_{i=1}^{N_i} (N_i - \widehat{\theta}_i)^2/\widehat{\theta}_i$, is presented in plots (d) of Fig. 13. Furthermore, the required critical values for the significant level of $\alpha = 0.01$ with the degree of freedom (df) 6 and 3 are also presented in the same plot.

As presented in the figure, the chi-square value at $i = 8$ (see plot (d) Fig. 13) exceeds the required critical value (i.e. ${\chi_{0.01}}^2$) for the significant level of $\alpha = 0.01$ with $df = 6$. Therefore, the predicted system events in the proposed failure intensity model in (2) with the respective parameters in (36) are slightly deviated from the actual system events for data interval II. However, the chi-square value at $i = 5$ (see plot (d) Fig. 13), is below the required critical value, ${\chi_{0.01}}^2$, for the significant level of $\alpha = 0.01$ with $df = 4$.. Therefore, the predicted system events in the failure intensity model in (2) with the respective parameters in (28) (i.e. Model 2) have satisfied the actual system events for a section (i.e. from 10,307.5 (Hrs) to 18,000 (Hrs)) of data interval II. One can observe that the gas turbine engine has encountered another multiple failure situation approximately at the system age of 18,923 (Hrs) (see Fig. 9) and that has introduced another erroneous region in the COHs. Hence, Model 2 of the gas turbine engine has satisfied the Cramer-Von Mises goodness-of-fit test until the system age of 18,923 (Hrs). It is recommended that this erroneous data interval should also be removed from the COHs and the proposed process should be repeated for data interval II.

4. Conclusions

This study focuses on system reliability analysis of an offshore power plant with several gas turbine engines, where the failure intensity of a selected gas turbine engines under varying maintenance actions is quantified, realistically. The proposed reliability models can be used to observe the system availability of the respective offshore power plant under condition based inspections and maintenance. The models are developed by the following steps:

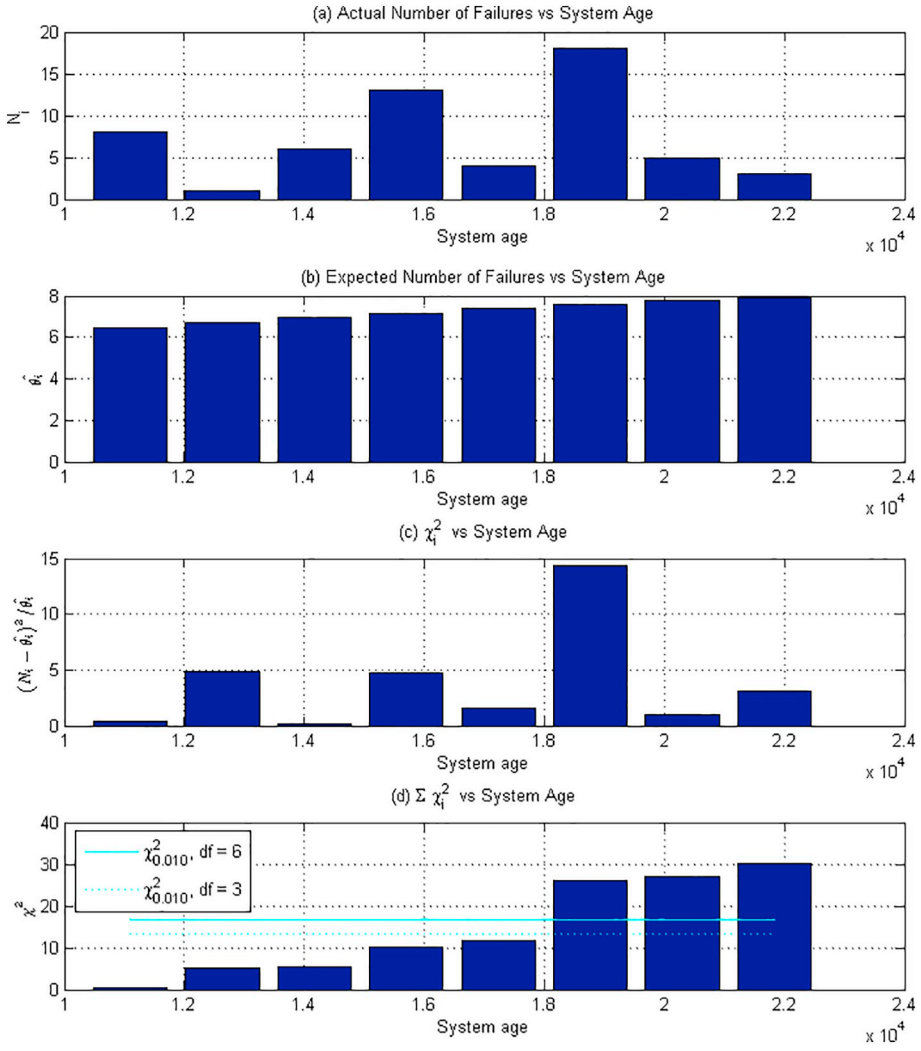

Fig. 13:. Chi-square statistics.

- Firstly, a failure transition diagram for the respective gas turbine is derived.
- Secondly, the failure intensity, i.e. mathematical model, of a selected gas turbine engine is estimated by removing the erroneous data conditions from the event data set of the same.
- Thirdly, the model satisfactory on a goodness- of-fit test is also evaluated to observe its accuracy.
- Fourthly, the same failure intensity model is used to calculate the meantime between failures (MTBF) and mission reliability values.

The proposed approach consists of a combination of several statistical analysis methods to overcome various erroneous data conditions (i.e. in event data) that may create many challenges in estimating the system reliability of offshore gas turbine engines. Such erroneous data conditions can degrade the parameter estimation process of the failure intensity models and those data regions should be removed before the parameter estimation process. The different sectors of the system life of a gas turbine engine may have different failure intensity values [45,46] due to the reasons that are discussed, previously and such situations can be observed by the LTT. It is also assumed that the system failures are recovered by a same number of repairs with negligible time periods in these models. This assumption is introduced to develop appropriate failure intensity models in gas turbine engines. However, some variations among actual and predicted system failures are observed (i.e. system model uncertainties), therefore such assumptions should be re-visited to understand those system-model uncertainties.

It is also noted that these system-model uncertainties (i.e. the failure intensity variations) can occur due to several factors: repeated start-up and shutdown failures, component failures [49–51] and various maintenance actions [52]. Therefore, these factors can introduce some erroneous data regions into system events and that can create several failure intensity levels in different sectors of the system life. The required measures should be taken to overcome such situations as proposed in this study, where the erroneous

regions should be identified and properly isolated from the system event data under so called “multi-interval data analysis”. Then, the modified system event data can be used to estimate the respective parameters of the failure intensity models of a selected gas turbine engine, where multiple models are derived with respect to several failure intensity levels in different sectors of the system life.

Finally, these models are tested with the respective goodness-of-fit tests to evaluate the actual and predicted failures of the gas turbine engine. This methodology should continue until the failure intensity models satisfy the goodness-of-fit tests and that eventually derives better models with multiple failure rates to predict system failure events. It is also noted that unknown maintenance actions (i.e. various repairs) may disturb the failure intensity of a gas turbine engine and these maintenance information can also play a crucial role in system failure behavior. These failure intensity levels with the respective maintenance information should be compared to evaluate the success of the respective maintenance actions. Furthermore, that (i.e. the maintenance information) can also be compared with the respective failure transition probabilities (see Fig. 7) to evaluate the past and present maintenance policies of the respective gas turbine engines.

Acknowledgement

This work is supported by the Center for Integrated Operations (IO) in the Petroleum Industry, Trondheim, Norway, under the project of Remaining Useful Life (RUL) Modeling for Gas Turbine Engines, System Integrity and Dynamic Risk Assessment (T3) and funded by the Research Council of Norway (NRC) and Petróleo Brasileiro S.A. (Petrobras).

References

[1] J. Wang, J.B. Yang, P. Sen, T. Ruxton, Safety based design and maintenance optimisation of large marine engineering systems, Appl. Ocean Res. 18 (1) (1996) 13–27.
[2] O. Michelsen, Use of reliability technology in the process industry, Reliab. Eng. Syst. Saf. 60 (1998) 179–181.
[3] N. Vedachalam, S. Muthukrishna Babu, G.A. Ramadass, M.A. Atmanand, Review of maturing multi-megawatt power electronic converter technologies and reliability modeling in the light of subsea applications, Appl. Ocean Res. 46 (June 2014) 28–39.
[4] ISO 14224, Petroleum, Petrochemical and Natural Gas Industries - Collection and Exchange of Reliability and Maintenance Data for Equipment, Second Edition, (2006) ISO 14424:2006(E).
[5] ISO 13380, Condition Monitoring and Diagnostics of Machines - General Guidelines on using Performance Parameters, (2002) ISO 13380:2002(E).
[6] C. Evans, D. Rees, D. Hill, Frequency-domain identification of gas turbine dynamics, Contr. Syst. Technol. IEEE Trans. 6 (5) (1998) 651–662.
[7] S. Garg, Aircraft Turbine Engine Control Research at NASA Glenn Research Center, Technical Report NASA/TM-2013-217821, NASA Glenn Research Center, Cleveland, OH, USA, April, 2013.
[8] F.J.G. Carazas, G.F.M. de Souza, Reliability analysis of gas turbine, in: G.F.M. de Souza (Ed.), Thermal Power Plant Performance Analysis, Springer Series in Reliability Engineering, London, 2012.
[9] Rolls-Royce, Rb211 Gas Turbine for Oil and Gas Applications, Houston, Texas, USA (2005).
[10] J.S. Litt, D.L. Simon, C. Meyer, H. DePold, J.R. Curtiss, H. Winston, Y. Wnag, I. Statler, Y. Gawdiak, NASA aviation safety program aircraft engine health management data mining tools roadmap, 14th Annual International Symposium on Aerospace/Defense Sensing, Simulation and Control AeroSense, 2000, pp. 24–28.
[11] T.V. Berikin, G.G. Kulikov, V.Y. Arkov, P.J. Fleming, Dynamic modeling for condition monitoring of gas turbines: Genetic algorithm approach, Proceedings of the 16th IFAC World Congress, 2005, pp. 739–742.
[12] X. Pu, S. Liu, H. Jiang, D. Yu, Sparse Bayesian Learning for Gas Path Diagnostics, J. Eng. Gas Turbines Power 135 (7) (Jun 12, 2013) 071601.
[13] R. Whalley and M. Ebrahimi, "Automotive gas turbine regulation," Contr. Syst. Technol. IEEE Trans., vol. 12, no. 3, pp. 465–473.
[14] D. Simon, D.L. Simon, Aircraft turbofan engine health estimation using constrained Kalman filter, J. Eng. Gas Turbines Power 127 (2) (2005) 323–328.
[15] D.L. Simon, Propulsion Diagnostic Method Evaluation Strategy (ProDiMES) User's Guide, NASA-TM-2010-215840, NASA, Glenn Research Center, Cleveland, Ohio, USA, 2010.
[16] A.J. Volponi, Gas turbine parameter corrections, J. Eng. Gas Turbines Power 121 (October, 1999) 613–621.
[17] J.S. Litt, D.L. Simon, S. Gang, T.H. Guo, C. Mercer, R. Millar, A. Behbahani, A. Bajwa, D.T. Jensen, A Survey of Intelligent Control and Health Management Technologies for Aircraft Propulsion Systems, NASA-TM - 2005-213622, ARL-TR-3413 NASA, Glenn Research Center, Cleveland, Ohio, USA, 2005.
[18] M.D. Espana, Sensor biases effect on the estimation algorithm for performance-seeking controllers, J. Propuls. Power 10 (4) (July–Aug, 1994) 527–532.
[19] G.B. Gilyard, J.S. Orme, Performance seeking control program overview and future directions, NASA Technical Memorandum, 4531 1993.
[20] J.S. Orme, S. Schkolnim, Flight assessment of the onboard propulsion system model for the performance seeking control algorithm on a f-15 aircraft, NASA Technical Memorandum, 4705 1995.
[21] G.S. Alag, G.B. Gilyard, A proposed Kalman filter algorithm for estimation of unmeasured output variables for an f100 turbofan engine, NASA Technical Memorandum 4234 (1990).
[22] D.L. Simon, S. Garg, Optimal Turner Selection for Kalman Filter-based Aircraft Engine Performance Estimation, Turbo Expo, 2009 ASME.
[23] L.P. Perera, P. Oliveira, C. Guedes Soares, Vessel detection, tracking, state estimation and navigation trajectory prediction for the vessel traffic monitoring and information process, IEEE Trans. Intell. Transp. Syst. 13 (3) (2012) 1188–1200.
[24] L.P. Perera, Navigation vector based ship Manoeuvring prediction, J. Ocean Eng. 138 (2017) 151–160.
[25] D. Xuewu, G. Zhiwei, T. Breikin, W. Hong, Disturbance attenuation in fault detection of gas turbine engines: a discrete robust observer design, Syst. Man Cyber. Part C: Appl. Rev. IEEE Trans. 39 (2) (March 2009) 234–239.
[26] M. Rausand, A. Hoyland, System Reliability Theory, Models Statistical Methods and Applications, 2nd Edn, John Wiley & Sons, Inc., Hoboken, New Jersey, USA, 2004.
[27] M. Basso, L. Giarre, S. Groppi, G. Zappa, NARX models of an industrial power plant gas turbine, Contr. Syst. Technol. IEEE Trans. 13 (4) (July 2005) 599–604.
[28] A.K.S. Jardine, P.M. Anderson, D.S. Mann, Application of the Weibull proportional hazards model to aircraft and marine engine failure data, Qual. Reliab. Engng. Int. 3 (1987) 77–82.
[29] F.P. dos Santos, A.P. Teixeira, C. Guedes Soares, Maintenance planning of an offshore wind turbine using stochastic petri nets with predicates, ASME 2013 32nd International Conference on Ocean, Offshore and Arctic Engineering (OMAE2013–11639), Nantes, France, June, 2013.
[30] H. Mikat, A.M. Siddiolo, M. Buderath, Virtual Framework for Validation and Verification and Verification of System Design Requirements to Enable Condition based Maintenance, 1st European Conference of the Prognostics and Health Management Society, 2012, pp. 225–238.
[31] G.P. Sallee, Performance deterioration based on existing (historical) data, JT9D Jet Engine Diagnostics Program, NASA-CR-135448, 1978.
[32] M.M. Machado, D.A.P.M. Manguinho, A. Valland, S. Ushakov, D. Roverso, W.H.A. Beere, RUL modeling for turbo generators of a FPSO: alternatives and challenges, Proceedings of the Rio Oil & Gas Expo and Conference, Rio de Janeiro, Brazil. (IBP 1802 14), 2014.
[33] M. Wall, R. Lee, S. Frost, Offshore Gas Turbines (and Major Driven Equipment) Integrity and Inspection Guidance Notes, Research report 430 ESR Technology Ltd, Oxforshire, UK, 2006.

[34] E. Chiodo, D. Lauria, Some basic properties of the failure rate of redundant reliability systems in industrial electronics applications, IEEE Trans. Ind. Electron. 62 (8) (Aug 2015) 5055–5062, https://doi.org/10.1109/TIE.2015.2404306.
[35] C.J. Kim, S.J. Lee, S.H. Kang, Evaluation of Feeder Monitoring Parameters for Fault Detection using Laplace Trend Statistics, 40(6) (2004), pp. 1718–1724.
[36] L.H. Crow, Evaluating the reliability of repairable systems, Reliability and Maintainability Symposium, Proceedings, Annual, 1990, pp. 275–279.
[37] G. Pulcini, Modeling the failure data of a repairable equipment with bathtub type failure intensity, Reliab. Eng. Syst. Saf. 71 (2001) 209–218.
[38] L.H. Crow, Reliability Analysis for Complex Repairable Systems. AMSAA Technical Report No. 138, U.S. Army Materiel Systems Analysis Activity, Aberdeen Proving Ground, Maryland, 1975.
[39] Jozef Van Dyck, Tim Verdonck, Precision of power-law NHPP estimates for multiple systems with known failure rate scaling, Reliab. Eng. Syst. Saf. 126 (June 2014) 143–152.
[40] I.J. Myung, Tutorial on maximum likelihood estimation, J. Math. Psychol. 47 (2003) 90–100.
[41] S.A. Smith, S.S. Oren, Reliability growth of repairable systems, Naval Res. Log. Quart. 27 (4) (December, 1980) 539–547.
[42] L.H. Crow, Reliability Analysis for a Complex Repairable Systems, Reliability and Biometry Statistical Analysis of Life Length, SIAM, Philadelphia, 1974, pp. 379–410.
[43] AMSAA Reliability Growth Guide, Technical Report No. TR-652, September, U.S. Army Materiel Systems Analysis Activity, Aberdeen Proving Ground, Maryland, USA, 2000.
[44] L.H. Crow, Confidence Interval Procedures for Reliability Growth Analysis. AMSAA Technical Report No. 197, U.S. Army Materiel Systems Analysis Activity, Aberdeen Proving Ground, Maryland, USA, June, 1977.
[45] L.P. Perera, M.M. Machado, A. Valland, D.A.P. Manguinho, System reliability of offshore gas turbine engines with erroneous data conditions, Proceedings of the 25th European Safety and Reliability Conference (ESREL 2015), Switzerland, September, 2015, pp. 1679–1688.
[46] L.P. Perera, M.M. Machado, A. Valland, D.A.P. Manguinho, Modelling of system failures in gas turbine engines of offshore platforms, Proceedings of the 2nd IFAC Workshop on Automatic Control in Offshore Oil and Gas Production, Florianpolis, Brazil, 2015, pp. 200–205.
[47] R. Venkatesan, G. Vengatesan, N. Vedachalam, M. Arul Muthiah, R. Lavanya, M.A. Atmanand, Reliability assessment and integrity management of data buoy instruments used for monitoring the Indian Seas, Appl. Ocean Res. 54 (January 2016) 1–11.
[48] L.H. Crow, A.P. Basu, Reliability Growth Estimation with Missing Data. II. Reliability and Maintainability Symposium, Proceedings, Annual IEEE, (1988), pp. 248–253.
[49] B. Cai, L. Huang and M. Xie, "Bayesian networks in fault diagnosis," in IEEE Trans. Ind. Info., Vol. 13, No. 5, pp. 2227–2240, Oct. 2017.
[50] L.P. Perera, B. Mo, Ship speed power performance under relative wind profiles in relation to sensor fault detection, J. Ocean Eng. Sci. (2018), https://doi.org/10.1016/j.joes.2018.11.001.
[51] Baoping Cai, Hanlin Liu, Min Xie, A real-time fault diagnosis methodology of complex systems using object-oriented Bayesian networks, Mech. Syst. Signal Process. 80 (2016) 31–44.
[52] R.B. Chinnam, On-line reliability estimation for individual components using statistical degradation signal models, Qual. Reliab. Engng. Int. 18 (2002) 53–73.